NASA
Technical Memorandum 87076

USAAVSCOM
Technical Report 85-C-15

Theoretical Modeling of the Vapor Cavitation in Dynamically Loaded Journal Bearings

David E. Brewe
Propulsion Directorate
U.S. Army Aviation Research and Technology Activity (AVSCOM)
Lewis Research Center
Cleveland, Ohio

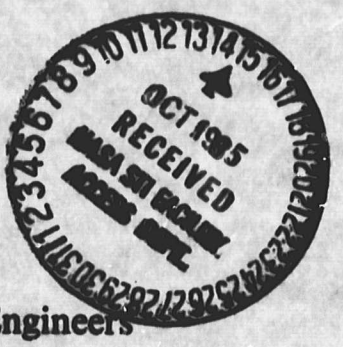

Prepared for the
Tribology Conference
cosponsored by the American Society of Lubrication Engineers
and the American Society of Mechanical Engineers
Atlanta, Georgia, October 8-10, 1985

NASA

THEORETICAL MODELING OF THE VAPOR CAVITATION IN DYNAMICALLY LOADED JOURNAL BEARINGS

David E. Brewe
Propulsion Directorate
U.S. Army Aviation Research and Technology Activity (AVSCOM)
Lewis Research Center
Cleveland, Ohio

ABSTRACT

A theoretical investigation is made of the evolution of a vapor bubble for a submerged journal bearing under dynamically loaded conditions. The solution to the Reynolds equation is determined numerically using a control volume method (Elrod algorithm). This method conserves mass throughout the computational domain including the liquid-vapor interface which may or may not be in motion relative to the minimum film line. An ADI (Alternating Direction Implicit) method is used to effect the time march. Excellent agreement was found with the experimental work of Jakobsson and Floberg for stationary cavitation. Predictions of bubble life for nonstationary cavitation compare reasonably well with that measured by Jacobson and Hamrock using high-speed photography. A comparison study was performed to determine some of the consequences of applying a nonconservative theory to a dynamic problem. A complete dynamic cycle of a journal whirling in a circular path was chosen for the basis of comparison. Significant differences were observed in the load components near the end of the cycle. In each case, onset of cavitation was observed followed by bubble growth and subsequent collapse. More complete details of this phenomena are illustrated with the use of perspective graphic plots depicting the associated pressure distribution and region of cavitation with position and motion of the journal within the housing.

NOMENCLATURE

D	shaft diameter, m
e	eccentricity, m
F_R	radial load component, N
F_φ	tangential load component, N
F_μ	friction force due to shear stress, N
g	switch function (cavitation index)
H	dimensionless film thickness, $h/\Delta R$
h	film thickness, m
L/D	length to diameter ratio
M	bearing torque, N-m
$\dot{m}_x, \dot{m}_z$	lineal mass flux, kg/m-s
P_L	power loss, N-m/s
p	fluid pressure, N/m^2
p_a	ambient pressure, N/m^2
p_c	cavitation pressure, N/m^2
p_o	dimensionless pressure, $p(\Delta R)^2/(R^2\mu\omega)$
R	radius of shaft, m
ΔR	radial clearance, m
t	time, s
U	sum of the surface velocities in x-direction, m/s
$\vec{V}$	sum of the surface velocity vectors, m/s
W	load capacity, N
w	squeeze-velocity, m/s
x	coordinate along circumference, m
Δx	incremental spacing along circumference, m
y	coordinate normal to x, z-plane, m
z	axial coordinate, m

Δz	axial incremental spacing, m
β	liquid bulk modulus, N/m^2
γ	angular position of minimum film, rad
ε	eccentricity ratio, $e/\Delta R$
μ	dynamic viscosity, $N\text{-}s/m^2$
ρ_c	fluid density within cavitated zone, kg/m^3
φ	angular coordinate relative to minimum film line, rad
φ_1	angular location of upstream cavitation boundary, rad
φ_e	angular location of downstream cavitation boundary, rad
θ	fractional film content in cavitation zone; density ratio (ρ/ρ_c) in full film zone
ω_d	orbital angular velocity of journal center about fixed point relative to housing center, rad/s
ω_s	angular velocity of journal about its own center, rad/s
ψ	attitude angle, tan (F_φ/F_R), rad
τ_x	shear stress for an oil element, N/m^2

INTRODUCTION

Machine elements in relative motion separated by a lubricating fluid can often be subjected to conditions which causes the fluid to cavitate. This cavitation can either be a result of (1) dissolved gas coming out of solution or (2) evaporation (flashing) of the fluid. Both types of cavitation are commonly observed in journal bearings, squeeze-film dampers, connecting rod bearings, and pistons. It has a pronounced effect on their operation. The occurrence of cavitation in journal bearings is shown (1) to result in reduced power loss, friction coefficient, bearing torque, and load capacity. Dowson and Taylor (2), in an excellent review of cavitation, point out that cavitation need not have a deleterious effect on the load-carrying capacity of bearings. Horsnell's predictions (3) on load capacity for steady-state

conditions show that consideration of cavitation can lead to a threefold increase over the predicted load if it is not considered.

In recent years, imposing higher loads and speeds together with more complicated loading cycles resulted in bearings experiencing "cavitation erosion-damage" (4). This damage occurs under conditions of vapor cavitation. The vapor pressure for most lubricating oils is very nearly zero. Very large implosive forces are created and confined to a small area as the vapor bubble collapses. The net effect is that metal is hammered out of the bearing surfaces by a fatigue process, resulting in erosion damage to the bearing surfaces. This phenomenon arises under conditions of dynamic loading and is frequently observed in main or crankshaft bearings in compression-ignition engines.

Aside from the cavitation damage, there is the damage that can occur due to self-excited instabilities that are encountered under dynamic loading. These instabilities can be manifested as a whirling or whipping motion (5) of the journal center. Large vibrational amplitudes can result in large forces being transmitted to the system. A designer can circumvent this problem, or at least the severity of it, by knowing the speed threshold at which it occurs. This information is often obtained by referring to "stability maps" (6,7). Stability maps require the determination of hydrodynamic force terms coupled to the dynamical equations of motion.

The calculation of the hydrodynamic force components is dependent on the film model used, especially at high eccentricities. Many of the film models that are used to generate stability maps involve theories that are overly restrictive (i.e., narrow bearing theory, infinite bearing theory) and treat the cavitation in a very superficial way. Notable of these is the π-film cavitation theory in which positive pressures extend through half the circumference of the bearing and the other half is regarded as cavitated.

Specifying zero-pressure gradient and cavitation pressure at the boundary (i.e., Swift-Stieber boundary conditions) represents the conditions for film rupture in a reasonable way but does not properly represent the conditions when the film is reestablished. In actual practice, the Swift-Stieber conditions are often compromised as a matter of convenience by neglecting the implementation of the zero-pressure gradient condition. This is much like the Gümbel conditions in which solutions were obtained to the Reynolds equation and cavitation was determined by disallowing the existence of subambient pressures. However, dynamic loading causes changes in the local film thickness which leads to nonstationary cavitation - that is, the cavitation boundary is in motion. This motion is manifested as growth and collapse of the bubble as well as downstream transport from the minimum film position. The appropriate boundary condition may require a condition other than a zero-pressure gradient at the boundary. The studies of Olsson (8,9) suggest that the usual Swift-Stieber film-rupture condition is adequate for dynamic situations if the cavitation boundary moves at a speed that is less than half the journal surface speed. It seems highly unlikely that this condition would be met during the initial stages of growth and the last stages of bubble collapse.

Jakobsson-Floberg (1) and Olsson (8) formulated boundary conditions for a moving boundary that conserved mass within the cavitated region as well as at the boundary (commonly referred to as the JFO cavitation theory). It was assumed that liquid was convected through the cavitated region in the form of striations extending to both surfaces in the film gap. There is evidence that some liquid is transported in the form of an adhered layer to the faster surface (10,11). Pan (12) has broadened the JFO theory to accommodate those situations in which the mass transport through the cavitated region is not necessarily via liquid striations. For moderately to heavily loaded bearings

(i.e., the load carrying capacity >> surface tension forces of the lubricant), the adhered layer can be neglected (10). The striated flow in the JFO theory is necessarily a Couette flow because of a constant pressure assumption within the cavitated region. Floberg's experimental findings (1) support the constant pressure assumption. However, Etsion and Ludwig (11) have measured pressure variations of the order of 50 kPa inside a gaseous cavitation bubble. To resolve this apparent contradiction, it seems that one must make the distinction of whether or not the cavitation bubble is gaseous or vaporous. Etsion (11) provides a plausible mechanism based on liberation and reabsorption rates between a gas and a liquid. The same arguments for pressure variation within a vapor bubble would not apply (cf. 13). In view of this discussion, the constant pressure assumption for vapor cavitation seems reasonable. Despite some of the controversy and certain lack of understanding, the JFO theory perhaps represents one of the best accounts of a dynamical theory to date for moderately to heavily loaded journal bearings and/or dampers. It is an improvement over the Swift-Stieber conditions, even for steady-state solutions, because it provides for film reformation or fillback as well as film rupture. Both rupture and fillback require a knowledge of the pressure gradient and fractional film content at the interface to determine its location. Unlike a rupture boundary, the fillback boundary is subjected to a pressure flow (i.e., nonzero pressure gradient). Furthermore, the fractional film content at the boundary is determined by a residual fluid within the cavitated region that has been released at a rupture boundary (earlier in time) and governed by the fluid transport law. Which condition (fillback or rupture) prevails depends on the relative motion of the boundary with the motion of the convected fluid normal to the boundary. Typically, under steady-state cavitating conditions, the rupture boundary occurs along the upstream boundary and the fillback boundary occurs along the downstream

end. Under dynamic loading and nonstationary cavitation, rupture or fillback conditions may be required at either the upstream or the downstream boundary. To effect these conditions in a computational algorithm, the programming task is exceedingly tedious, and this discourages their implementation in current practice.

Elrod and Adams (14) introduced a computational scheme that mimics the JFO theory. It avoids the complex programming required to trace the moving boundary between grid points and evaluating the required pressure derivative. Later, Elrod (15) modified it and presented it in more detail. The algorithm incorporates a switching function that "switches out" any pressure flow within the cavitated region. This automatically introduces a cavity conforming to the requirements of mass continuity and the JFO theory. Elrod has compared results generated by the algorithm with experimental results of Lundholm (16) for steady-state operation of a circumferentially fed journal bearing. The results (i.e., cavitation extent, load capacity, and attitude-angle versus eccentricity) were quite good. To the author's knowledge, a limited few (17,18) have used the algorithm for steady-state applications. No one to date has explored the full intended capabilities of the algorithm, that is, a dynamically loaded application.

It is the purpose of this paper to analyze a dynamically loaded journal bearing through its entire periodic motion. The prescribed motion of the journal relative to the bearing will be undergoing circular whirl to conform with the experimental work of Jacobson and Hamrock (13,19). Comparison of predicted bubble life to that measured by Jacobson and Hamrock (13) will be discussed. Furthermore, results obtained from using an often used nonconservative theory (i.e., pseudo-Gümbel BC) are compared with the Elrod algorithm.

BACKGROUND THEORY

Elrod and Adams (14) implemented a moving boundary scheme that avoids interface complications. The following is a review of some of the underlying factors that lead up to the algorithm which was later modified by Elrod (15) and used here. The conservation of mass can be written as

$$\frac{\partial(\rho h)}{\partial t} + \vec{\nabla} \cdot \dot{\vec{m}} = 0 \tag{1}$$

where $\dot{\vec{m}}$ represents the lineal mass flux and is given by

$$\dot{\vec{m}} = \rho \frac{h\vec{V}}{2} - \frac{\rho h^3}{12\mu} \vec{\nabla} p \tag{2}$$

Substituting Eqs. (2) into (1) leads to the Reynold's lubrication equation. This equation has been made applicable to the cavitation region as well as the full film region by incorporating a switch function to automatically satisfy the boundary conditions at a moving interface. Furthermore, the fractional film content θ has been made the dependent variable. This required giving θ a dual interpretation. That is, in the full film region, θ represents the mass content of the film that exceeds the content that would exist if the pressure were at cavitation pressure p_c. In other words,

$$\theta = \rho/\rho_c \tag{3}$$

where ρ_c is the density of the liquid at the pressure p_c. Furthermore, p and ρ are related through the equation for the liquid bulk modulus according to

$$\rho \frac{\partial p}{\partial \rho} = \beta \tag{4}$$

or

$$p = p_c + \beta \ln \theta \qquad \theta \geq 1.0 \tag{5}$$

In the cavitation region ($\theta \leq 1.0$) θ determines the mass content ($\rho_c \theta h$) which can manifest itself in the form of a smeared mass or striated flow extending to both surfaces in the film gap. The fluid transported through the cavitation region in the form of an adhered film can be neglected for heavily loaded conditions.

A universal differential equation is made possible by linking the solutions of the full film region with the solutions in the cavitated region via a single dependent variable θ. However, a cavitation index, or switch function g, was included so that the resulting PDE would be consistent with the uniform pressure assumption within the cavitated region. The switch function is defined from a knowledge of θ. Thus,

$$\left.\begin{aligned} g &= 0 \qquad \theta < 1.0 \\ g &= 1 \qquad \theta \geq 1.0 \end{aligned}\right\} \tag{6}$$

and g is made a factor of the pressure gradient term in Eq. (2) so that the flow is strictly Couette in the cavitated region. Expressing the lineal mass flux $\vec{\dot{m}}$ in terms of θ and g and substituting it into Eq. (1) result in the universal differential equation obtained in Ref. 14; i.e.,

$$\frac{\partial(\theta h)}{\partial t} + \frac{\vec{V}}{2} \cdot \vec{\nabla}(\theta h) = \vec{\nabla} \cdot \frac{h^3}{12\mu} \beta g(\theta) \vec{\nabla}\theta \tag{7}$$

In the full film region the solutions of θ together with Eq. (5) determine the pressures. In the cavitation region, $g = 0$, and Eq. (7) becomes

$$\frac{\partial(\theta h)}{\partial t} + \frac{\vec{V}}{2} \cdot \vec{\nabla}(\theta h) = 0 \tag{8}$$

which governs the transport of the fluid through the cavitation region.

NUMERICAL ALGORITHM

The numerical scheme is based on the Elrod algorithm (15) in which mass is conserved throughout the computational domain. This method combines a control volume (CV) approach to deriving the finite-difference equations with the use

of a switching function to automatically satisfy the boundary conditions at a moving interface. A CV is constructed about each nodal point in space (Fig. 1) to implement the conservation property in the differencing scheme. A computational cell of this sort requires evaluations of variables and their derivatives to be carried out at the cell faces. Variables at the cell faces are determined to be the simple arithmetic mean between its adjacent nodal values at a time t. The derivatives are evaluated by centered differences. With this preamble, the conservation law is stated as follows:

$$\left\{\begin{array}{l}\text{The total increase of}\\ \text{mass } (\rho_c h\theta) \text{ in the CV}\\ \text{over a time } \Delta t\end{array}\right\} = \left\{\begin{array}{l}\text{The net lineal mass flux}\\ \text{of } (\rho_c h\theta) \text{ into the CV by}\\ \text{convection plus the net}\\ \text{lineal mass flux of } (\rho_c h\theta)\\ \text{into the CV by diffusion}\end{array}\right\}$$

This translates to

$$(\Delta \times \Delta z)\frac{\partial(\rho_c \theta h)}{\partial t} = \dot{m}_x \Delta z + \dot{m}_z \Delta x \tag{9}$$

which is equivalent to Eq. (1). The treatment of the lineal mass flux is the crux of the Elrod algorithm and the essence of it is as follows. Considering for the moment one direction, namely x, then

$$\dot{m}_x = (\dot{m}_x)_{\text{convection}} + (\dot{m}_x)_{\text{pressure}} \tag{10}$$

Convective Contribution

The switch function g is judiciously applied to the convective term at the upstream cell face to give

$$\dot{m}_{x-\Delta x/2} = \frac{\rho_c U}{2}\left[\theta_{-1}h_{-1}(1 - g_{-1}) + g_{-1}h_1 + g_o g_{-1}(h_o - h_{-1})/2\right] \tag{11}$$

The subscripts refer to the nodal position relative to the CV (see Fig. 1). Eq. (11) is well defined in that it is self-consistent with the CV approach and retains the physics as well. The lineal mass flux at the downstream face

is obtained by suitably reassigning the subscripts of Eq. (11). Thus the incremental change to the lineal mass flux due to convection is

$$(\dot{\Delta m}_x)_{conv} = \left[\frac{\rho_c U}{2} h_{-1}(1 - g_{-1})\theta_{-1} - h_0(1 - g_0)\theta_0 + \frac{g_{-1}h_{-1}}{2}(2 - g_0) + \frac{g_0 h_0}{2}(g_{-1} - 2 + g_1) - \frac{g_1 h_1 g_0}{2}\right] \quad (12)$$

An attractive feature of this expression is that in the full film region (all $g = 1$) the factor $\partial(h\theta)/\partial x$ that appears in the convective term is central differenced, retaining second-order accuracy. In the cavitation region, the algorithm accounts for the mass transport consistent with conservation properties by including θ in the derivative (i.e., $\partial(h\theta)/\partial x$). The role of the switch function automatically effects an upwind differencing scheme for the evaluation of this term, thereby retaining properly posed conditions at the boundaries as time is advanced.

Pressure Gradient Contribution

The Poiseuille or pressure gradient contribution to the lineal mass flux at the upstream face is

$$(\dot{m}_{x-\Delta x/2})_{press} = -\frac{\overline{h^3 \rho_c}}{12\mu} g(\theta)\left(\overline{\frac{\partial p}{\partial x}}\right)_{x-\Delta x/2} \quad (13)$$

where the bar represents the average value at the indicated cell face. The pressure is determined from θ by the approximation to Eq. (5),

$$p \simeq p_c + \beta(\theta - 1) \quad (14)$$

Central differencing the pressure at the upstream cell face and making use of the previous equation one obtains

$$(\dot{m}_{x-\Delta/2})_{press} = -\frac{\overline{h^3 \rho_c}}{12\mu} \beta \frac{g_0(\theta_0 - 1) - g_{-1}(\theta_{-1} - 1)}{\Delta x} \quad (15)$$

The lineal mass flux due to diffusion that is leaving the CV at the downstream end is

$$(\dot{m}_{x+\Delta x/2})_{press} = -\frac{\overline{h^3\rho_c}}{12\mu}\beta\frac{g_1(\theta_1 - 1) - g_0(\theta_0 - 1)}{\Delta x} \qquad (16)$$

In this analysis we do not need to represent h^3 by an averaging method. We can evaluate it exactly. Thus, the net lineal flux into the CV by diffusion is

$$(\dot{\Delta m}_x)_{press} = \frac{\rho_c\beta}{12\mu}\left[\frac{h^3_{-1/2}g_{-1}(\theta_{-1} - 1) - (h^3_{-1/2} + h^3_{+1/2})g_0(\theta_0 - 1)}{\Delta x} + \frac{h^3_{+1/2}g_1(\theta_1 - 1)}{\Delta x}\right] \qquad (17)$$

If all three points are within the cavitation zone, then $\dot{\Delta m}_x = 0$. This is consistent with the zero pressure gradient assumption in that region. If all three points are in the full film zone, then Eq. (17) reduces to a central differencing scheme for the pressure gradient. There are numerous interpolative combinations that occur at the boundary using Eqs. (12) and (17), all of which make up the boundary conditions automatically and consistent with mass conservation from grid point to grid point.

Time March

The time march related to Eq. (1) must now be considered. In this study, an alternating direction implicit (ADI) scheme was applied. The implicit Euler method was used to advance the time at each half time step since this is known to be unconditionally stable (20) insofar as the ordinary differential

equation is stable. For the first half time step, a differencing along the circumference is performed; that is,

$$\left.\begin{aligned} (h\theta)^{t+\Delta t/2} - (h\theta)^{t} &= \frac{\Delta t}{2\rho_c}\left(\frac{\Delta \dot{m}_x}{\Delta x}^{t+\Delta t/2} + \frac{\Delta \dot{m}_z}{\Delta x}^{t}\right) \\ \text{or} \qquad \left(h\theta - \frac{\Delta t}{2\rho_c}\frac{\Delta \dot{m}_x}{\Delta x}\right)^{t+\Delta t/2} &= \left(h\theta + \frac{\Delta t}{2\rho_c}\frac{\Delta \dot{m}_z}{\Delta z}\right)^{t} \end{aligned}\right\} \tag{18}$$

During the next half time step, the axial direction is differenced giving

$$\left.\begin{aligned} (h\theta)^{t+\Delta t} - (h\theta)^{t+\Delta t/2} &= \frac{\Delta t}{2\rho_c}\left(\frac{\Delta \dot{m}_x}{\Delta x}^{t+\Delta t/2} + \frac{\Delta \dot{m}_z}{\Delta z}^{t+\Delta t}\right) \\ \text{or} \qquad \left(h\theta - \frac{\Delta t}{2\rho_c}\frac{\Delta \dot{m}_x}{\Delta x}\right)^{t+\Delta t} &= \left(h\theta + \frac{\Delta t}{2\rho_c}\frac{\Delta \dot{m}_x}{\Delta x}\right)^{t+\Delta t/2} \end{aligned}\right\} \tag{19}$$

Solutions

The previous equations lead to two systems of equations that can be represented by a periodic tridiagonal matrix B_p in the circumferential sweep and a tridiagonal matrix B for the axial sweep. In other words, we can represent Eq. (18) as

$$\sum_i B_p^{ij}\, \theta_i^{t+\Delta t/2} = C^{j,t} \tag{20}$$

Because of the periodic or wrap-around boundary conditions, B_p^{ij} takes the form

$$B_p^{ij} = \begin{pmatrix} b_1 & c_1 & & & a_1 \\ a_2 & b_2 & c_2 & 0 & \\ & a_3 & b_3 & c_3 & \\ & & \ddots & \ddots & \ddots \\ & 0 & & \ddots & \ddots \\ c_k & & & a_k & b_k \end{pmatrix} \tag{21}$$

The solutions of θ along the circumference are found by performing a Gauss-Jordan reduction on B_p using a maximum-pivot strategy to reduce the error. The solutions obtained by differencing along the axial direction are more readily obtained by using a nonpivoted Gaussian elimination procedure (tridiagonal solver). Since the journal and housing are aligned, the pressures must be symmetric about the axial center. Consequently, the calculations are only made over half the axial length of the housing.

Switch Function

The switch function was updated after each half-time step. Occasionally, during the collapse of the vapor bubble, liquid was piling up at the boundary. It appears that the switch function was not accommodating the movement of the boundary adequately for that time step (21). Consequently, the switch function was immediately updated and the calculation was reiterated.

RESULTS AND DISCUSSION

A numerical scheme based on the Elrod algorithm was devised to study vapor cavitation in a submerged journal bearing for both steady and dynamic loading. The method conserves mass throughout the computational domain including the region of cavitation. In this investigation, the algorithm was checked against published experimental data. Furthermore, an analysis of a journal whirling in a circular path through one orbit was then performed. The consequences of applying a nonconservative theory (pseudo-Gümbel boundary conditions) in lieu of the conservative Elrod algorithm are determined.

Experimental Comparison

Steady state. - Jakobsson and Floberg (1) have measured pressures within a submerged journal bearing operating at steady-state conditions with cavitation. The operating conditions for the particular experiment chosen as a basis of comparison are given in Table I. These conditions were used as input to the computer code. Figure 2 illustrates the bearing configuration

along with the predicted steady-state pressure distribution that resulted from the author's numerical calculations using the Elrod algorithm. The journal is rotating in a counterclockwise direction. Thus, the entrainment velocity through the minimum film is in a counterclockwise direction, and by convention considered positive. The line of centers forms a horizontal which extends through the position of minimum film thickness. The positive pressures seen in the three-dimensional plot are generated in the converging clearance region below this horizontal line. In the direction of rotation, the pressures become subambient in the diverging clearance region above the horizontal. The upstream and downstream meniscus of the cavitation boundary is outlined there. The corresponding extent of cavitation is shown by the outline of asterisks in the three-dimensional plot.

Pressures were measured along the circumference of the bearing at two axial positions relative to the axial center in Ref. 1. Figure 3 compares the predicted pressures using the Elrod algorithm with these experimental data. The vertical axis is a measure of the dimensionless pressure p_0 and the horizontal axis represents the circumferential position (in rad) relative to the minimum film line. In general, the agreement appears quite good. The extent of cavitation determined experimentally can be seen to be greater than the numerical solution at both positions. Furthermore, there appears to be a slight discrepancy at the position of peak pressure. These discrepancies did not appear to adversely affect the agreement between the predicted and experimentally determined load capacity. The predicted load (2147 N) came to within 4.6 percent of that measured in Ref. 1 (2250 N).

Dynamic loading. - For practical considerations, very little work has been done on submerged journal bearings in dynamically loaded conditions. This is because submerged journal bearings with ambient supply pressure require the existence of subambient pressures to remain operative. Otherwise, the flow

balance into and out of the bearing cannot be maintained, especially if a portion of the duty cycle is steady state. The fluid must be degassed so that the gaseous cavitation that might otherwise form at near ambient pressure does not preclude the formation of subambient pressure.

Jacobson and Hamrock (13,19) have studied vapor cavitation in a submerged journal bearing. In their studies, a high-speed motion picture camera was used to capture the cavitation formation and collapse under dynamically loaded conditions. Figure 4 illustrates the configuration used in the tests. The bearing (housing) vibrated in a circular motion keeping the axis of vibration parallel to the axis of rotation. The journal could be rotated about its own fixed center in space. The dynamic conditions chosen as a basis of comparison are stated in Table I. The important result of Ref. 13 insofar as this study is concerned is the observance of the complete life cycle of vapor cavitation. High-speed photography revealed that, for the conditions listed in Table I, the vapor bubble remained visible for at least 23 ms. This represented approximately one-third of the full dynamic cycle of the bearing.

The predicted life of the vapor bubble from the computer code was 32 ms. A part of this difference arises because this measure of bubble life inherently contains a certain time duration for which the computer indicates cavitation although in reality it would be invisible to the eye. This is probably not the major contributing factor to the discrepancy, however. The pressures calculated for these conditions were of the order of 10^7 N/m^2. A plastic (polymethylmethacrylate, PMMA) was used as a housing material for viewing purposes. It is thus most likely that deformation effects are responsible for the discrepancy not accounted for by the numerical method. Furthermore, the experiment allowed the eccentricity to reach a maximum value of 1.0, whereas a certain amount of numerical instability was observed when the eccentricity exceeded 0.98. Consequently, the input conditions for the

computations were not identical to the input conditions of the experiment. Future experiments are planned so that comparison between theory and experiment can be more conclusive.

Comparison of Two Theoretical Models

Motion. - The conservative cell method (Elrod algorithm) is compared with a nonconservative scheme (psuedo-Gümbel BC) to analyze the effects of vapor cavitation in a dynamically loaded journal bearing. The prescribed motion (Table I) of the journal center was in a clockwise circular orbit (-92.7 rad/s) about a point fixed in space relative to the bearing center. The journal spun (-19.5 rad/s) in the clockwise direction about its own axis, which was considered parallel to the axis of the bearing housing. The net result for this motion is a positive entrainment velocity (Fig. 4) which, by convention, is in the counterclockwise direction. A complete orbit took a total of 66.7 ms. The instantaneous eccentricity ϵ increased from an initial value of 0.1 to a maximum of 0.8 during the squeeze action of the journal (first half cycle). During journal separation (remaining half cycle), it returned to its initial value of 0.1.

Cavitation and pressure distribution. - The results obtained by using the Elrod algorithm (Fig. 5) are compared with those obtained from the often used psuedo-Gümbel (see the appendix) boundary conditions (Fig. 6). Figures 5 and 6 illustrate the similarities and differences of the pressure distribution as they occur throughout the entire orbit. Figures 5(a) and 6(a) represent the position of the journal within the housing and the associated pressure distribution at the initial instant in time. The pressure buildup due to the combined squeezing and sliding motion of the journal is shown for the first half cycle in Figs. 5(a) to (d) and 6(a) to (d). It should be noted when comparing parts (c) and (d) that the maximum peak pressure does not occur when the eccentricity is a maximum as one might first expect. This can be

explained by referring to Fig. 7 and noting that the squeeze velocity approaches zero and the sliding velocity approaches a minimum at the end of the half cycle. This offsets the effectiveness of generating increasing pressures due to a decreasing film. The onset of cavitation occurs between parts (c) and (d), 27 ms into the cycle. The squeeze component is known to suppress the conditions for cavitation (22). Note that in Figs. 5(d) and 6(d), the pressure distribution and the extent and position of the vapor bubble are distinctly different. The conservation algorithm of Elrod predicts a slightly higher pressure peak and a smaller vapor bubble, which begins about 15° further downstream from the minimum film line. Proceeding from (d) to (e) shows the journal (near the minimum film line) separating from the bearing. The initial stages of separation creates a suction effect, causing the pressure hump to dissipate and the vapor bubble to expand. Note that parts (b) and (e) were both generated at the same value of eccentricity. The essential difference is that the squeeze velocity has a different sign; that is, when the squeeze velocity is negative (the clearance is decreasing), the motion of the journal is producing a squeeze effect (part (b)). In part (e), the squeeze velocity is positive (i.e., the clearance is increasing) and produces a suction. In comparing Figs. 5(e) with 6(e) the difference in bubble size has become even more noticeable. Here we see in both cases that the vapor bubble has actually crossed the minimum film line and been drawn into the converging clearance space of the bearing. This effect is greater for the nonconservative theory. As the journal continues to pull away from the bearing, the increased clearance means that a much greater Poiseuille side flow is present to cause the collapse of the bubble. This is because the Poiseuille side flow is proportional to h^3. In both theories, the bubble drifts downstream from the minimum film line and collapses. The Elrod algorithm predicts a much longer bubble life (8.4 ms) with an oblong shaped

bubble that actually crosses the maximum film line before collapsing. This collapse occurs about 7 ms into the succeeding orbit.

Bearing film calculations. - The effects of boundary conditions on bearing film calculations are shown in Fig. 8. The calculations derived from the nonconservative model (dotted lines) are superimposed on the curve derived from the conservative model (solid line). The load capacity and load components are shown in Figs. 8(a) to (f) as a function of the eccentricity during a full period of shaft whirl. The letter callouts on the plots can be used as chronological indicators since they refer to the parts in Figs. 5 and 6 chronologically. The load-eccentricity plots might well be described as "journal bearing hysteresis loops." For increasing ϵ the W-ϵ curve is entirely different from that for decreasing ϵ. That is, proceeding from part (a) to part (d), ϵ is increasing and the squeeze velocity is always negative. During this initial half-cycle, cavitation is for the most part absent. For decreasing ϵ, the squeeze velocity is always positive and cavitation is almost always present. The drastic loss in load capacity in going from part (c) to (d) is a result of the journal motion (Fig. 7) and the development of cavitation close to the minimum film line. The negative pressures in the diverging clearance tend to cancel the positive pressures in the converging clearance. However, the motion is perhaps the major factor influencing the drastic load loss.

As should be expected, differences from the boundary conditions appear only when cavitation is present. At the higher eccentricities ($0.5 < \epsilon < 0.75$), the largest difference in load capacity is about 10 percent. The radial load component accounts for the largest part of this deviation. Again this is because the vapor bubble is located close to the minimum film. In fact, in the discussion of Figs. 5 and 6 it was pointed out that the bubble actually penetrated the region of converging film. Note that

a larger bubble leads to a reduction in the load components. The reverse effect is noted for the total load capacity. This is because the magnitudes of the load components are the important factors and not the relative values when determining total load (see the appendix). As the eccentricity continues to decrease, the dotted and solid lines tend to converge, except in the case of the tangential load. In this plot, these two lines continue diverging until the journal begins its next orbit. In the nonconservative theory the bubble has collapsed just 1 ms before the journal returns to its initial position. By contrast, the vapor bubble plays a very active role in the load characteristics well into the next orbit, according to the conservative theory. As the bubble penetrates the maximum film, the radial load once again becomes the dominant factor in the deviations due to boundary conditions. These deviations represent as much as a 20-percent difference in the total load capacity. The dramatic dip in load during the initial stage of the second orbit and each succeeding orbit is due to the sudden collapse of the vapor bubble. The hysteresis loops are repeatable insofar as the circular orbit of the journal is maintained.

The attitude angle is an angular measure between the load line and the line of centers. It is defined in the appendix along with the film force calculations. The effect of the boundary conditions on the attitude angle is seen only when the eccentricity is decreasing. This effect results from the differences in extent and location of the bubble.

The bearing torque and power loss in the bearing show no boundary condition effect except perhaps on a fine scale. The only differences in making these calculations are in the handling of the shear stress in the cavitated region. Since pressure gradients are assumed not to exist there, the shear stress arising from the Couette flow must reflect any possible differences. This calculation is directly proportional to the fractional film

content in the vapor region and the extent of the vapor region. In the case of the nonconservative theory, the fractional film content is not calculated. Therefore, it must either be assumed to be entirely vapor or filled with oil. These calculations were made assuming the zero pressure region, which has a linear velocity distribution, is filled with oil. According to Figs. 8(e) and (f), this contribution was negligible for the scale shown.

CONCLUDING REMARKS

A theoretical investigation is made of the evolution of a vapor bubble for a submerged journal bearing under dynamically loaded conditions. The solution to the Reynolds equation is determined numerically using a control volume method (Elrod algorithm). This method conserves mass throughout the computational domain including the liquid-vapor interface which may or may not be in motion relative to the minimum film line. An ADI method is used to effect the time march.

Excellent agreement was found with the experimental work of Jacobson and Floberg (1) for stationary cavitation. A prediction of 32-ms bubble life for nonstationary cavitation was obtained from the dynamic theory for conditions (13) listed in Table I. Using high-speed photography for the same set of conditions, Jacobson and Hamrock observed a bubble life of 23 ms. This discrepancy was attributed to deformation effects as well as some uncertainty in correlating actual life with duration of visibility. Furthermore, the maximum eccentricity in the experiments was 1.0. Numercial instabilities prohibited eccentricities larger than 0.98. Future experiments are planned to preclude some of these problems so that comparison between theory and experiments can be more conclusive.

A comparison study was performed to determine some of the consequences of applying a nonconservative theory to a dynamic problem. A complete dynamic cycle of a journal whirling in a circular path was chosen for the basis of

comparison. Significant differences were observed in the load components near the end of the cycle. As much as a 20-percent difference in load capacity was observed. Differences in attitude angle were brought about by differences in extent and location of the bubble. Bearing torque and power loss were not affected by applying the pseudo-Gümbel boundary conditions in lieu of the dynamic theory.

In conclusion, the consequences of applying a nonconservative theory are noticeable only in the load components at the tail end and beginning of the journal orbit. The ease with which the Elrod algorithm can be implemented is an attractive feature. However, the present code consumes roughly 2 to 3 times the computational time of the Gümbel solutions when using a Gauss-Seidel iterative SOR scheme. Faster codes are available (i.e., fast Fourier transforms and multigrid codes) that could conceivably reduce the computational time by an order of magnitude. This certainly would make the algorithm a viable film model for rotor dynamic and squeeze-film damper applications.

APPENDIX

Film Force Calculations

The film forces are all determined here in much the same way as they were derived in Ref. 1. The tangential load component is a force acting normal to the line of centers at the minimum film position:

$$F_\varphi = - \iint_S p \sin\varphi \, R \, d\varphi dz \tag{A1}$$

The radial load acts along the line of centers:

$$F_R = \iint_S p \cos\varphi \, R \, d\varphi dz \tag{A2}$$

The total load and attitude angle can then be determined:

$$W = \sqrt{F_R^2 + F_\varphi^2} \tag{A3}$$

$$\psi = \tan^{-1}(F_\varphi / F_R) \tag{A4}$$

The friction force is determined from the shear stress τ_x:

$$F_\mu = \iint_S \tau_x \Big|_{y=h} R \, d\varphi dz \tag{A5}$$

For a film thickness h the shear stress is

$$\left.\begin{aligned} \tau_x \Big|_{y=h} &= \frac{h}{2}\frac{\partial p}{\partial x} + \mu \frac{U\theta}{h} \\ h &= \Delta R \, (1 - \varepsilon \cos\varphi) \\ H &= 1 - \varepsilon \cos\varphi \end{aligned}\right\} \tag{A6}$$

where

If one integrates the pressure gradient term by parts, then

$$F_\mu = \frac{\Delta R}{2} \int Hp \Big|_{\varphi_1}^{\varphi_e} dz + \iint_S \frac{\Delta R \varepsilon}{2} p \sin\varphi \, d\varphi dz + \frac{\mu U R}{\Delta R} \iint_S \frac{\theta}{H} \, d\varphi dz$$

$$= \frac{\Delta R}{2} \int Hp \Big|_{\varphi_1}^{\varphi_e} dz - \frac{\varepsilon \Delta R}{2R} F_\varphi + \iint_S \frac{\mu U}{\Delta R} \frac{\theta}{H} R \, d\varphi dz \tag{A7}$$

All integrations were performed using a Simpson's rule for single as well as double integrations.

Power Loss

The power loss can be obtained from the shear force, i. e.,

$$P_L = F_\mu U \tag{A8}$$

Bearing Torque

The bearing torque is given as

$$M = F_\mu R \tag{A9}$$

Pseudo-Gumbel Boundary Conditions

The Gumbel boundary conditions are often used as a substitute for the more rigorous Swift-Stieber rupture boundary conditions for reasons of computational economy. Normally the Gumbel conditions are implemented by first solving the Reynolds equation without any regard to cavitation. All subambient pressures are disallowed by setting them equal to the ambient pressure. This serves as the condition for cavitation. Note that the specification of the pressure gradient at the boundary is neglected. In this study, the nonconservative theory was not strictly in accord with Gumbel; that is, subambient pressures were allowed, and the vapor bubble was determined by disallowing pressures less than the cavitation pressure.

The numerical procedure used to implement the Gumbel conditions was the commonly used Gauss-Seidel iterative technique. This was done to provide a point of reference in assessing the penalty (if any) of invoking a more accurate theory.

REFERENCES

1. Jakobsson, Bengt, Floberg, Leif, "The Finite Journal Bearing Considering Vaporization," Trans. Chalmers Univ. Tech., Goteborg, No. 190, 1957.

2. Dowson, D. and Taylor, C.M., "Cavitation in Bearings," Ann. Rev. Fluid Mech., 1979, pp. 35-66.

3. Horsnell, R., McCallion, H., "Prediction of Some Journal-Bearing Characteristics Under Static and Dynamic Loading," Instn. Mech. Engrs., Lubrication and Wear Convention, 1963, pp. 126-138.

4. Wilson, R.W., "Cavitation Damage in Plain Bearings," 1st Leeds-Lyon Symp. Cavitation Relat. Phenom. Lubr., pp. 177-184, London, New york: Mech. Eng. Publ. Ltd.

5. Newkirk, B.L., "Shaft Whipping," Gen. Elec. Rev., Vol. 27, 1924, p. 169.

6. Badgley, R.H. and Booker, J.F., "Turborotor Instability Effect of Initial Transients on Plane Motion," J. Lubr. Technol., Vol. 91, Oct. 1969, pp. 625-633.

7. Kirk, R.G., Gunter,E.J., "Short Bearing Analysis Applied to Rotor Dynamics. Part I: Theory," J. Lubr. Technol., Vol. 98, January 1976, pp. 47-56.

8. Olsson, K.O., "Cavitation in Dynamically Loaded Bearings," Chalmers University of Technology, Goteborg, 1965.

9. Olsson, K.O., "On Hydrodynamic Lubrication with Special Reference to Nonstationary Cavitation," Chalmers University of Technology, Goteborg, 1974.

10. Coyne, J.C., Elrod, H.G., "Conditions for the Rupture of a Lubricating Film - Part II. New Boundary Conditions for Reynolds Equation," J. Lubr. Technol., Vol. 93, No. 1, January 1971, pp. 156-167.

11. Etsion, I.,Ludwig, L.P., "Observation of Pressure Variation in the Cavitation Region of Submerged Journal Bearings," J. Lubr. Technol., Vol. 104, April 1982, pp. 157-163.

12. Pan, C.H.T., "Dynamic Analysis of Rupture in Thin Fluid Films. I - A Noninertial Theory," J. Lubr. Technol., Vol. 105, January 1983, pp. 96-104.

13. Jacobson, B.O., Hamrock, B.J., "Vapor Cavitation in Dynamically Loaded Journal Bearings," C206/83, I. Mech. E., 1983, pp. 133-140.

14. Elrod, H.G., Adams, M.L, "A Computer Program for Cavitation and Starvation Problems," Cavitation and Related Phenomena in Lubrication, D. Dowson, M. Godet, and C.M. Taylor, eds., Mechanical Engineering Publications, Ltd., 1975, pp. 37-41.

15. Elrod, H.G., "A Cavitation Algorithm," J. Lubr. Technol., Vol. 103, July 1981, pp350-354.

16. Lundholm, Gunnar, "The Circumferential Groove Journal Bearing Considering Cavitation and Dynamic Stability," Acta Polytechnica Scandinavica, ME 42, Stockholm, 1969, pp. 1-89.

17. Lebeck, A.O., Teale, J.L., and Pierce, R.E., "Hydrodynamic Lubrication with Wear and Asperity Contacted in Mechanical Face Seals," Annual Report ME-86(78)Onr-414-1, prepared for the Office of Naval Research under Contract No. ONRN-00014-76-C-0071, Bureau of Engineering Research, The University of New Mexico, Albuquerque, N.M., Jan. 1978.

18. Miranda, A.A.S., "Oil Flow, Cavitation and Film Reformation in Journal Bearings Including an Interactive Computer-Aided Design Study," PhD Thesis, Univ. of Leeds, U.K., August 1983.

19. Jacobson, B.O., Hamrock, B.J., "High-Speed Motion Picture Camera Experiments of Cavitation in Dynamically Loaded Journal Bearings," J. Lubr. Technol., Vol. 105, July 1983, pp. 446-452.

20. Warming, R.F., Beam, R.M., "An Extension of A-Stability to Alternating Direction Implicit Methods," NASA TM-78537, 1978.

21. Elrod, H.G., private communication.

22. Ghosh, M.K., Hamrock, B.J., Brewe, D.E., "Hydrodynamic Lubrication of Rigid Nonconformal Contacts in Combined Rolling and Normal Motion," AVRADCOM TR 84-C-2; NASA TM 83578, 1984.

TABLE I. - OPERATING CONDITIONS

	Steady-state	Dynamic	
	Reference 1	Reference 13	Present study
ΔR	1.455×10^{-4} m	5.0×10^{-4} m	5.0×10^{-4} m
R	0.050 m	0.0425 m	0.0425 m
L/D	4/3	1/4	1.0
ε	0.61	0.32-1.0	0.1-0.8
ω_s	-48.1 rad/s	-19.5 rad/s	-19.5 rad/s
ω_d	0.0 rad/s	-92.7 rad/s	-92.7 rad/s
β	1.72×10^9 N/m^2	1.72×10^9 N/m^2	1.72×10^9 N/m^2
μ	0.0127 N-s/m^2	0.066 N-s/m^2	0.066 N-s/m^2
p_a	0.0 N/m^2	1.0133×10^5 N/m^2	1.0133×10^5 N/m^2
p_c	-72139.79 N/m^2	0.0 N/m^2	0.0 N/m^2

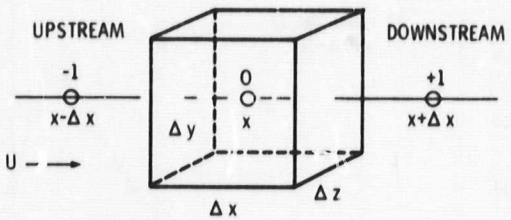

Figure 1. - Control volume CV at point x.

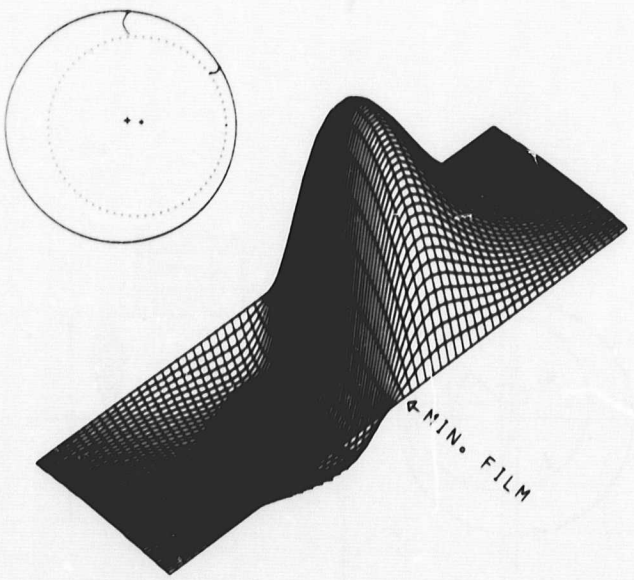

Figure 2. - Pressure distribution and bearing configuration using experimental conditions of Floberg (ref. 1).

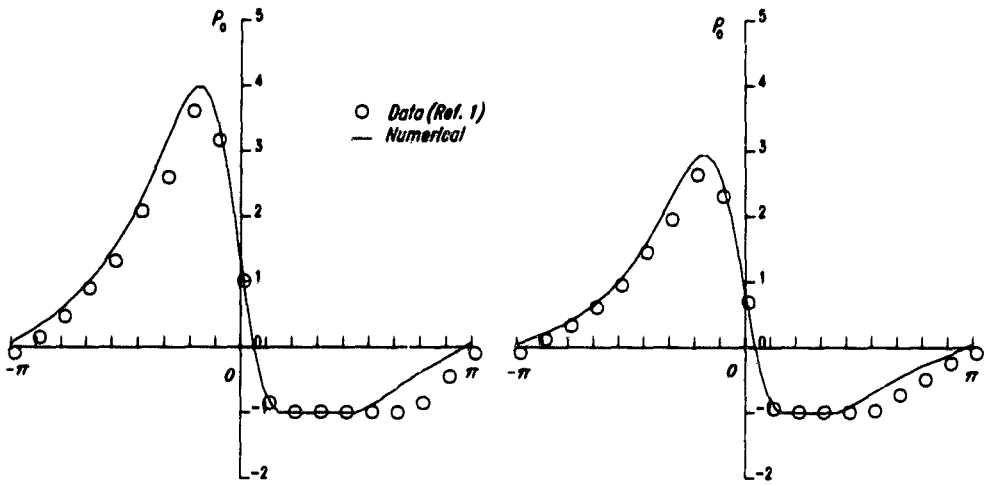

(a) Axial position from centerline (L/5D). (b) Axial position from centerline (3L/5D).

Figure 3. - Comparison of experimental to predicted pressures (dimensionless) along circumference.

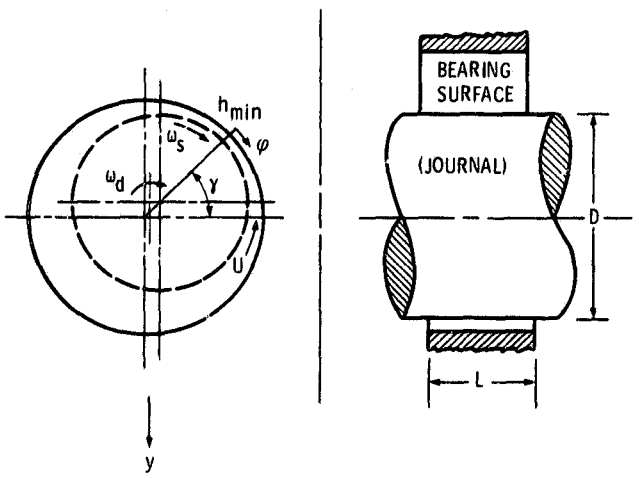

Figure 4. - Journal bearing configuration.

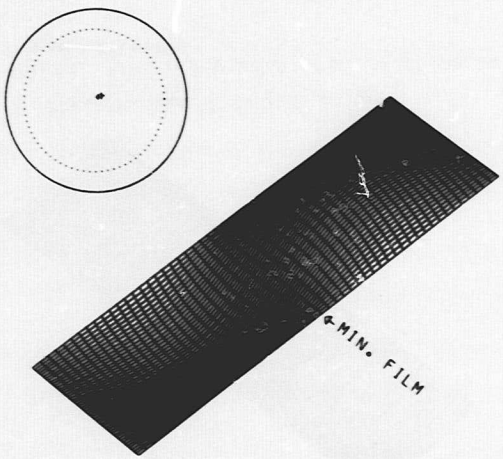

(a) Initial conditions (t = 0 ms; ε = 0.10).

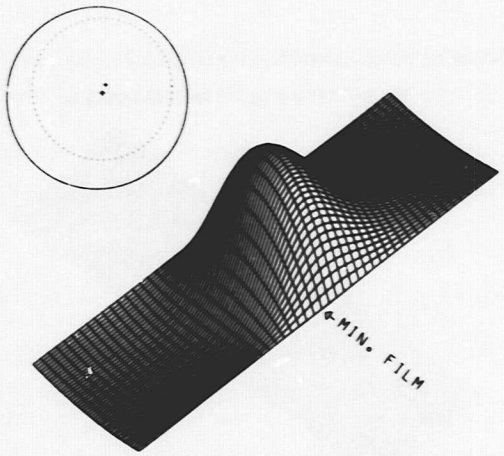

(b) Squeeze motion (c = 12.4 ms; ε = 0.50).

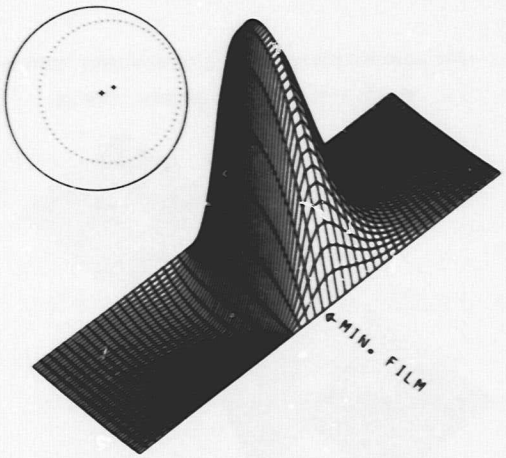

(c) Occurence of peak load (t = 25.3 ms; ε = 0.74).

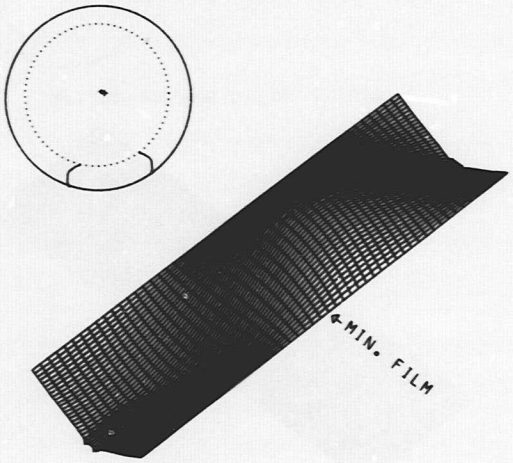

(f) Bubble collapse (t = 71.0 ms; ε = 0.16).

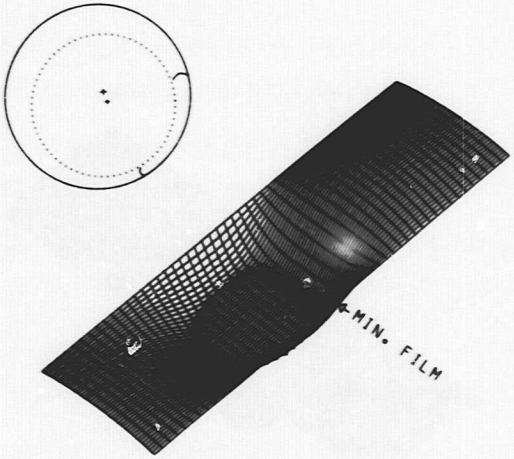

(e) Bubble expands (t = 53.4 ms; ε = 0.50).

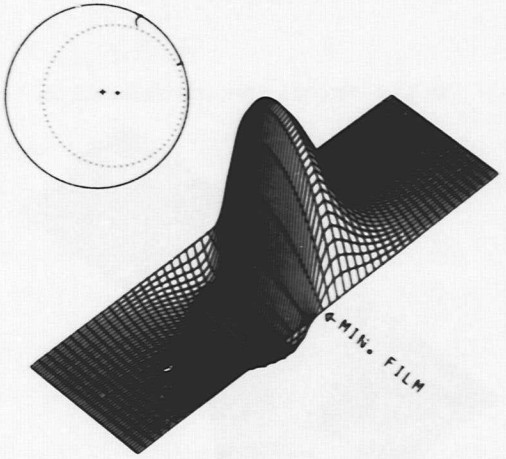

(d) Begin separation (t = 33.6 ms; ε = 0.80).

Figure 5. - Pressure distribution and bearing configuration for a full period of shaft whirl using Elrod's algorithm. Figures (a) to (f) viewed in clockwise are consecutive in time.

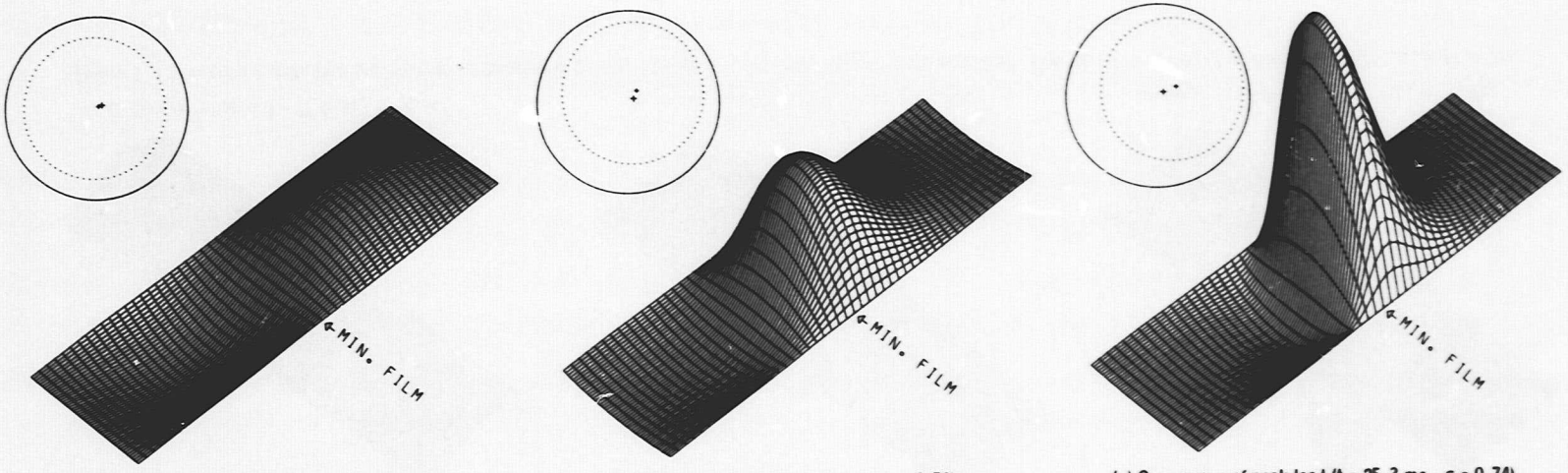

(a) Initial conditions (t = 0 ms; ε = 0.10).

(b) Squeeze motion (t = 12.4 ms; ε = 0.50).

(c) Occurance of peak load (t = 25.3 ms; ε = 0.74).

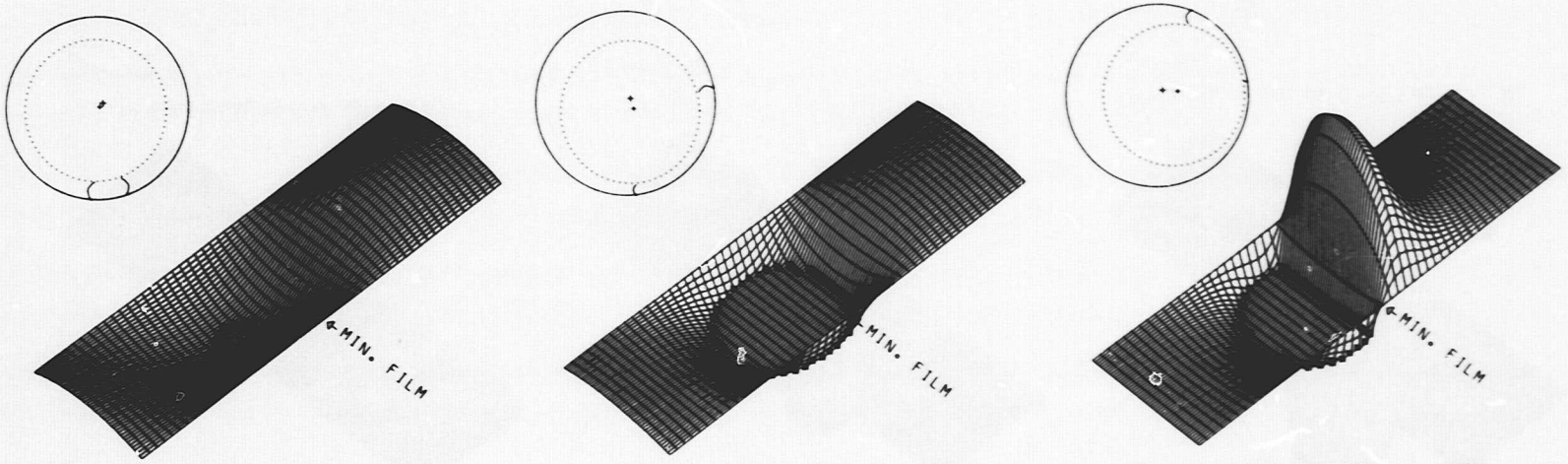

(f) Bubble collapse (t = 65.0 ms; ε = 0.14).

(e) Bubble expands (t = 53.4 ms; ε = 0.50).

(d) Begin separation (t = 33.6 ms; ε = 0.80).

Figure 6. - Pressure distribution and bearing configuration for a full period of shaft whirl using pseudo-Gümbel boundary conditions. Figures (a) to (f) viewed in clockwise order are consecutive in time.

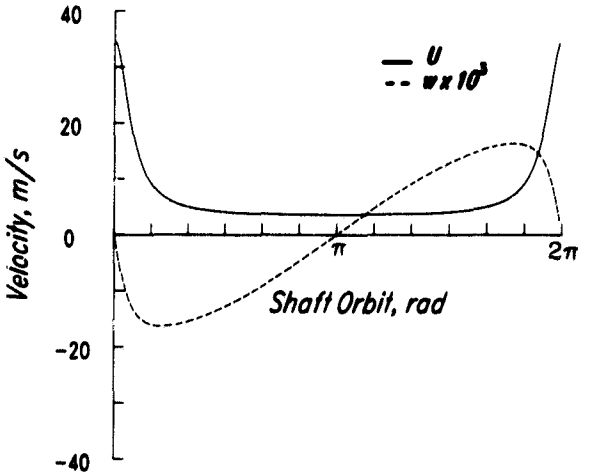

Figure 7. - Surface velocity sum (U) and squeeze velocity (w) during a full period of shaft whirl.

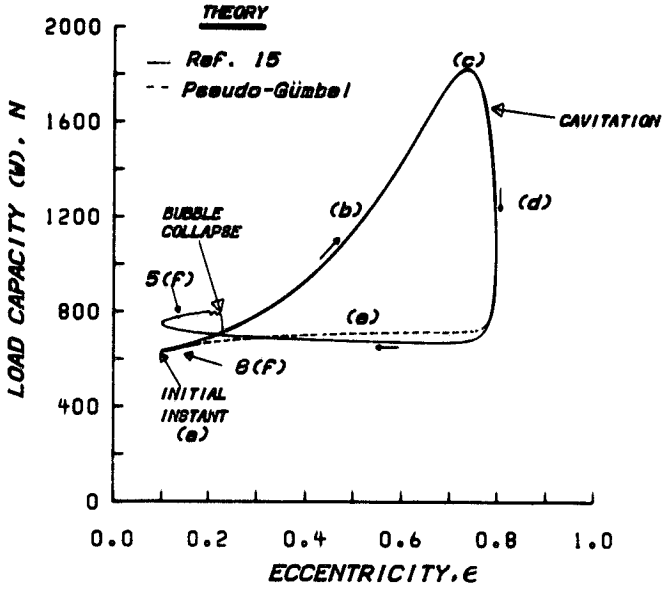

(a) Load capacity vs. eccentricity.

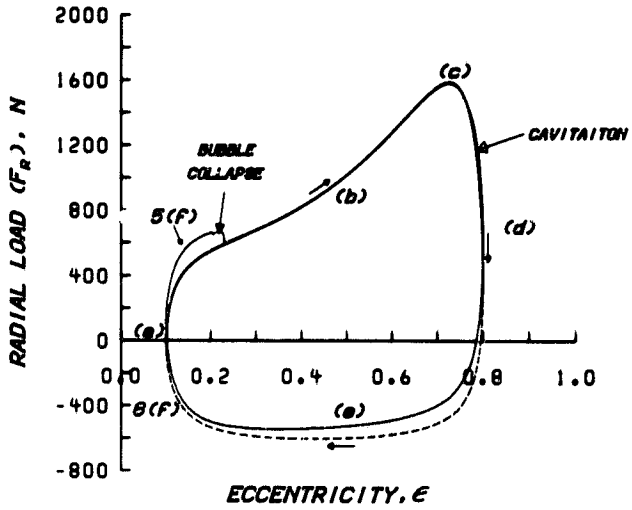

(b) Radial load vs. eccentricity.

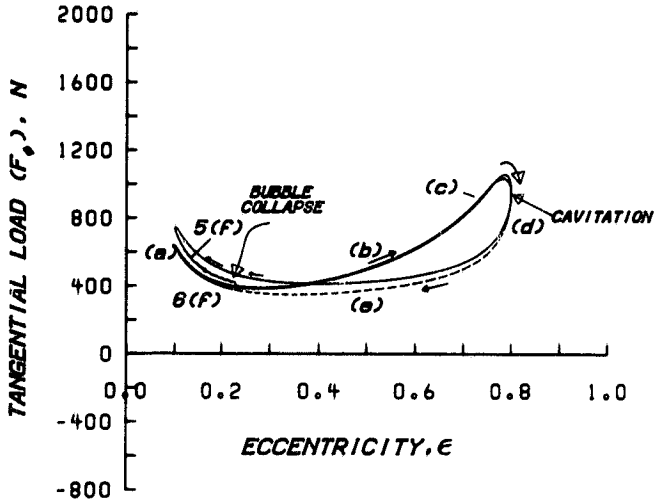

(c) Tangential load vs. eccentricity.

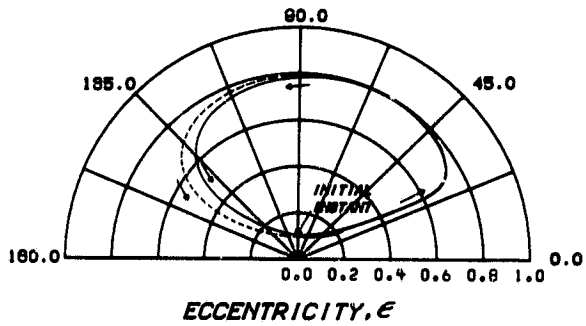

(d) Attitude angle vs. eccentricity.

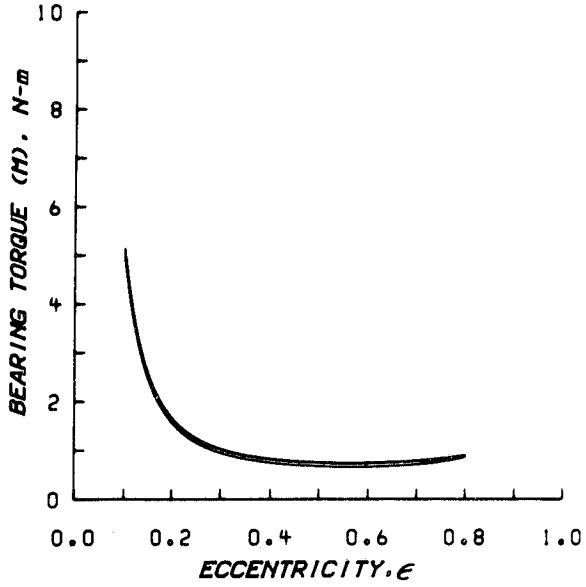

(e) Bearing torque vs. eccentricity.

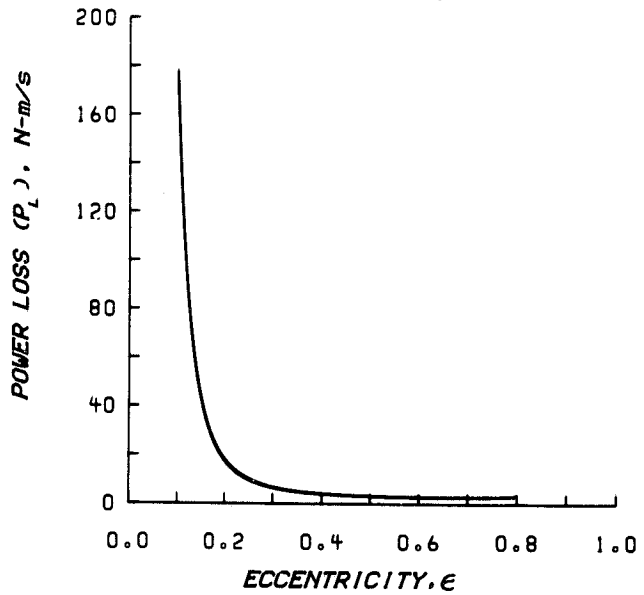

(f) Power loss vs. eccentricity.

Figure 8. - Effect of boundary conditions on film force calculations vs. eccentricity for a full period of shaft whirl.

1. Report No.	2. Government Accession No.	3. Recipient's Catalog No.
NASA TM-87076 USAAVSCOM-TR-85-C-15		

4. Title and Subtitle	5. Report Date
Theoretical Modeling of the Vapor Cavitation in Dynamically Loaded Journal Bearings	6. Performing Organization Code 505-33-62
7. Author(s) David E. Brewe	8. Performing Organization Report No. E-2651
	10. Work Unit No.
9. Performing Organization Name and Address NASA Lewis Research Center and Propulsion Directorate U.S. Army Aviation Research and Technology Activity (AVSCOM), Cleveland, Ohio 44135	11. Contract or Grant No.
	13. Type of Report and Period Covered Technical Memorandum
12. Sponsoring Agency Name and Address National Aeronautics and Space Administration Washington, D.C. 20546 and U.S. Army Aviation Systems Command, St. Louis, Mo. 63120	14. Sponsoring Agency Code

15. Supplementary Notes

Prepared for the Tribology Conference cosponsored by the American Society of Lubrication Engineers and the American Society of Mechanical Engineers, Atlanta, Georgia, October 8-10, 1985.

16. Abstract

A theoretical investigation is made of the evolution of a vapor-bubble for a submerged journal bearing under dynamically loaded conditions using the Elrod algorithm. This method conserves mass throughout the computational domain. A comparison study was performed to determine some of the consequences of applying a nonconservative theory (pseudo-Gümbel BC) to a dynamic problem. A complete dynamic cycle of a journal whirling in a circular path was chosen for the basis of comparison. Significant differences were observed in the load components near the end of the cycle. Further, good agreement with experiment is found for stationary and nonstationary cavitation.

17. Key Words (Suggested by Author(s))	18. Distribution Statement
Journal bearings; Cavitation; Dynamics; Vapor cavitation; Theoretical modeling; Switch function; Bubble dynamics; Vapor bubble; Whirl	Unclassified - unlimited STAR Category 34

19. Security Classif. (of this report)	20. Security Classif. (of this page)	21. No. of pages	22. Price*
Unclassified	Unclassified		

*For sale by the National Technical Information Service, Springfield, Virginia 22161